In-plane and out-of-plane characterization of a 3D angle interlock textile composite

F. Dau [a,*], M.-L. Dano [b], B. Vérone [b], J. Girardot [a], Z. Aboura [c], J.-M. Morvan [a]

[a] Institut de Mécanique et Ingénierie de Bordeaux (I2M), UMR CNRS 5295, Arts et Métiers Sciences et Technologies, Esplanade des arts et métiers, Talence 33405, France
[b] Université Laval, Département de génie mécanique, Pavillon Adrien-Pouliot, Québec G1V 0A6, Canada
[c] Laboratoire Roberval, UMR 7337, UTC Compiègne, Rue Roger Couttolenc, Compiègne 60200, France

A B S T R A C T

The present work focuses on the characterization of the in-plane and out-of-plane behavior of a three-dimensional angle-interlock woven composite. In-plane tensile and compression tests, short beam shear tests and through-the-thickness compressive tests were carried out to assess the mechanical behavior of the composite material. The results are presented in terms of stress–strain responses, elastic moduli, failure strains and strengths. In addition, the material elastic properties were measured using an ultrasonic method. Results are compared with the values of the elastic properties determined by mechanical testing. A good correlation is observed which demonstrates the pertinence of this technique to measure in particular the through-thickness elastic properties of the material.

1. Introduction

Composite materials are increasingly being used for primary aircraft components because of their superior structural performances such as high strength, high stiffness, long fatigue life, and lightweight. These structures are prone to impact loading during their service life. Conventional laminated composites have fibers oriented only in the plane of the laminate and therefore exhibit poor through-thickness mechanical performances. Three-dimensional (3D) woven composites in which through-the-thickness yarns are introduced offer significant advantages over conventional laminates. In particular, 3D composites do not exhibit delamination, prove better damage tolerance and superior impact performances [1]. Therefore, interest for using 3D woven composites for aircraft applications is growing.

In general, 3D woven composites consist of warp yarns that run in the machine direction (1-direction), weft yarns that run perpendicular to the machine direction (2-direction) and binder yarns that go through the thickness (3-direction). 3D woven composites can be divided in four types depending on the angle of the binder yarns and how deep the binder yarns penetrate in the fabric as shown in Fig. 1. If the angle is equal to 90°, the fabric is called orthogonal interlock (ORT) (Fig. 1a and Fig. 1b) whereas if the angle is less than 90°, the fabric is referred to angle interlock (AI) (Fig. 1c and Fig. 1d). If the binder yarns go through the entire fabric thickness, it is classified as through-thickness interlock (TT) (Fig. 1a and Fig. 1c) whereas if the binder yarns interlace with only a few layers, it is called layer-to-layer interlock (LTL) (Fig. 1b and Fig. 1d). The type of interlock fabric affects directly the unit-cell size and degree of crimp.

Much work has been done to characterize the mechanical behavior of various types of 3D woven composites along the warp and weft directions in tension [1–14], compression [2,3,9,11,14] or bending [2,3,9,14]. A few studies have also been reported on the off-axis (45°) behavior of 3D woven composite [3,6,7,8,11,13]. However, experimental studies to characterize the through-thickness properties of 3D woven composites are very scarce [8,14–16]. This is due to the lack of suitable and standardized test methods to investigate the through-thickness response of this kind of materials. 3D woven composites are usually thin. Increasing the thickness would require increasing the thickness of the preform, which would change the yarn architecture.

A comprehensive review of the available literature on the mechanical characterization of 3D woven composites has been published [17]. It highlights very clearly the knowledge gaps still present in the literature. The paper mentions in particular that the behavior of ORT interlock composites has been the most studied especially under in-plane tension and compression. Through-thickness angle-interlock (TTAI) composites have received much less attention although they were shown to

Corresponding author.
E-mail address: frederic.dau@ensam.eu (F. Dau).

outperform ORT woven composites [9]. Therefore, there is a need to characterize the mechanical behavior of TTAI architecture 3D composites subjected to warp, weft, 45° directions in-plane loading as well as through-thickness loading.

From the literature, it appears that the determination of the elastic properties has been performed through destructive mechanical tests. Researchers usually used strain gages [5,8,9], extensometers or digital image correlation (DIC) to measure the strains [8,9,11–13]. Although ultrasonic (US) methods have been used to characterize conventional laminates [18–21], it has so far not been applied to 3D woven composites. Therefore, there is a need to investigate the use of this technique to evaluate the elastic properties of 3D composites.

This paper focuses on the static characterization of a 3D angle-interlock woven composite. The objectives of the present work are to (1) characterize the in-plane and out-of-plane mechanical behavior of a 3D through-thickness angle-interlock composite (TTAI); (2) provide reliable and extensive data on a 3D angle-interlock composite to be used in numerical models; (3) assess the accuracy of ultrasonic methods to evaluate the elastic properties of 3D composites.

Experimental investigations are conducted to determine in-plane and out-of-plane elastic and failure properties of a 3D angle-interlock composite. No standard test methods have been specifically developed for 3D textile composites. In many cases, the usual standard test methods for traditional high performance composites can be used if proper specimen geometries and gage sizes are selected [22]. Depending upon the size of the yarns and the pattern of the weave, the inhomogeneity within a 3D textile composite can be quite large. In the case of 3D angle-interlock composites, the representative unit cell can be several dozen millimeter long. This implies, if the recommendations given in [22] are followed, to use very large specimens. In this work, various specimen sizes will be considered for the tensile tests to assess scale factors effect.

After describing the 3D angle-interlock composite studied in this work, in-plane tensile and shear tests conducted to determine the elastic modulus in both weft and warp directions and the shear modulus are first presented. Then, the results of in-plane compressive tests in the warp and weft directions are discussed. Next, the 3D angle-interlock composite was subjected to through-the-thickness compression and short-beam shear (SBS) tests. Full-field surface strain distributions obtained using a digital image correlation system are presented and discussed. Finally, the determination of the through-thickness elastic properties of the 3D angle-interlock composite using an ultrasonic method is presented. The results are then compared and discussed. Finally, general conclusions are drawn and prospects for future research conclude this work.

2. Material description

The present study focuses on a 3D angle-interlock woven composite already investigated by the authors for low velocity impact loading [23]. The fabric is composed of binding (or 3D) warp yarns, stuffer (or straight warp) yarns and filler (or weft) yarns as depicted in Fig. 2a. The ratio of 3D (binding) warp yarns to straight warp yarns is equal to 55%. The fabric has the same number of warp and weft yarns. The present fabric can be defined as a 3D warp interlock A-T 9–5 {5–4} according to the general definition of 3D warp interlock fabric referenced in [24]. Both the warp and the weft yarns were manufactured with carbon HR Tenax-E HTS40 F13 12 K 10Z yarns. The surface density is 2720 g/m^2. The fiber volume fraction is about 58.5 %. Fig. 2b shows a micro-computer-tomography (micro-CT) of the dry 3D angle-interlock woven fabric before being injected with resin.

The 3D angle-interlock woven fabric is then processed by Resin Transfer Moulding (RTM) using a RTM6 epoxy resin. The resin is injected at 120° C and the composite plate is cured at 160° C. The thickness of the dry interlock fabric is 10 mm before injection whereas the final thickness of the plates is 2.8 mm. The useful dimensions of the plates issued from the RTM process are 500 mm × 500 mm. The microstructure of the composite material was studied by performing micrographs of the plate cross sections. Fig. 3a and Fig. 3b illustrate the cross section of the composite along the warp and the weft directions, respectively. A binder warp yarn, running through the entire thickness is clearly visible in Fig. 3a. Fig. 3b shows that the weft yarns do no remain straight but wave significantly in a repetitive manner. The representative unit cell (RUC) could be determined from the micrographs and is represented by the red rectangles in Fig. 3. One can estimate that the unit cell has a thickness of 2.8 mm, a length of about 50 mm in the warp direction, and a width of about 10 mm in the weft direction.

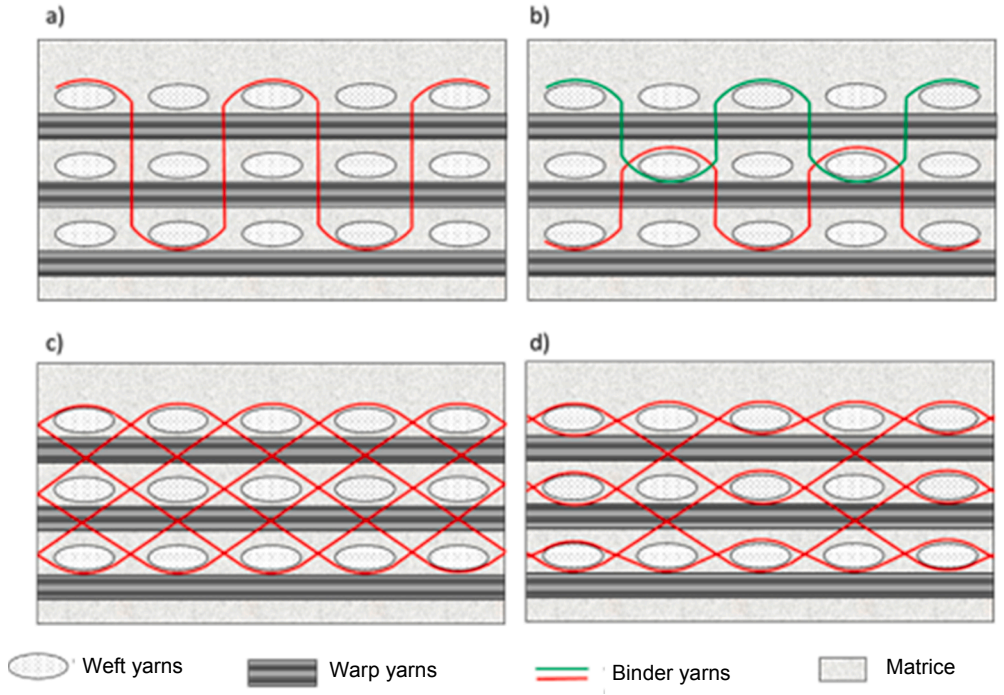

Fig. 1. Types of 3D woven composites: (a) Through-thickness orthogonal, (b) Layer-to-layer orthogonal, (c) Through-thickness interlock, (d) Layer-to-layer interlock.

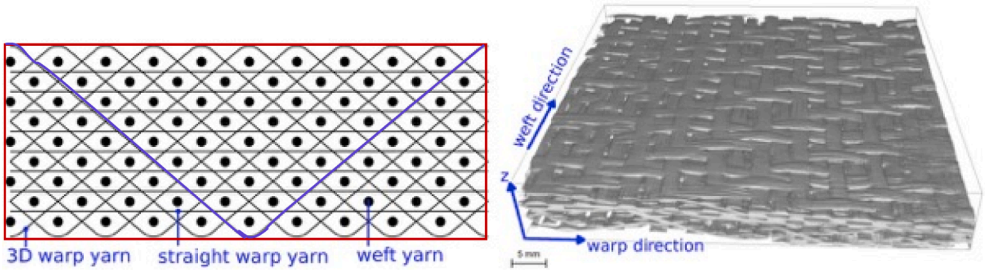

(a) Diagram of the cross section unit cell (b) Micro-CT scan

Fig. 2. 3D angle-interlock woven composite.

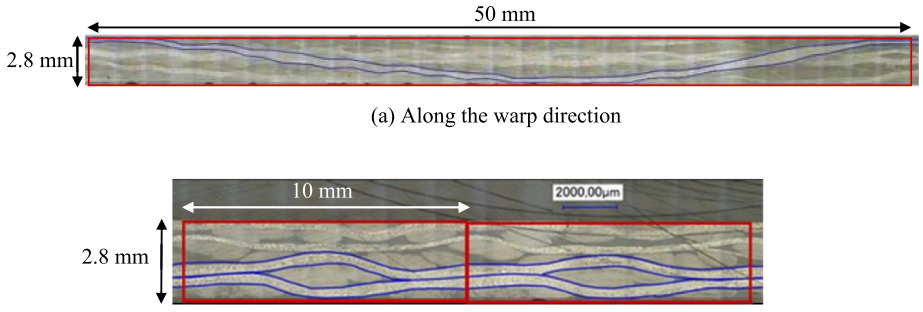

(a) Along the warp direction

(b) Along the weft direction

Fig. 3. Micrographs of the 3D angle-interlock woven composite cross section.

Fig. 4 shows a close-up of the interlaced weft and warp yarns. One can see that the fiber distribution within a yarn is uneven which is caused by compaction during the RTM process. Some resin rich areas are clearly visible and can take the form of paths within the yarn. As a consequence, the mechanical properties will probably exhibit some variations.

3. Characterization of the in-plane properties

Tensile tests along the weft and warp directions and in-plane shear tests were performed to determine the tensile Young modulus in the weft and warp directions, the in-plane Poisson ratio and the in-plane shear modulus, respectively. Compressive tests were also performed to measure the compressive Young modulus in the weft and warp directions.

3.1. Tensile tests along the weft and warp directions

3.1.1. Device and measurements

A Zwick tensile machine equipped with self-locking grips was used. The crosshead speed of the machine was set to 2 mm/min. The crosshead displacement of the machine and the loading force were recorded. A laser extensometer was used to measure the longitudinal strain. Video cameras were added to allow post-processing using digital image correlation. The images frequency was 1 Hz.

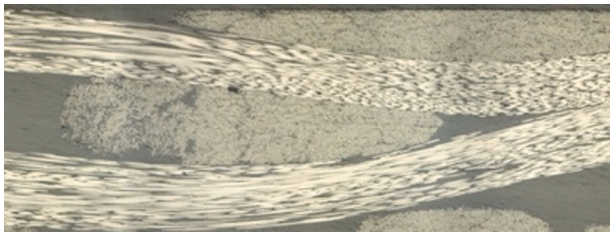

Fig. 4. Details of the 3D angle-interlock woven composite microstructure.

3.1.2. Scale effect study

As mentioned in section 2, the representative unit cell of the 3D angle-interlock composite has a length of about 50 mm in the warp direction, and a width of about 10 mm in the weft direction. In the ASTM Standard Guide for Testing Fabric-Reinforced "Textile" Composite Materials [22]. it is recommended to use a specimen geometry that contains at least two unit cells along the width. This implies that the width of the specimen should be 100 mm for the tensile tests in the weft direction. Since it is inconvenient to use such large specimens, a scale effect study is conducted to evaluate if it would be possible to use smaller specimens without compromising the results.

To assess the scale effect, tensile tests have been performed in the weft direction on specimens with two different geometries as shown in Fig. 5. The first one called "narrow" is of thickness 2.8 mm, out-of-grip length 180 mm and width 30 mm. The second one referred as "wide" has the same thickness but has an out-of-grip length of 340 mm and a width of 78 mm. It was not possible to test a specimen with a 100 mm width due to width limitation of the grips.

As depicted in Fig. 5, the representative unit cell is repeated many times along the length for the two specimens (weft direction). However, along the width (warp direction), the narrow specimen contains slightly over a half unit cell and the wide specimen about one and a half unit cell.

For both wide and narrow specimens, strains were obtained by digital image correlation. For the narrow specimens, only one camera was used whereas a second camera was necessary to capture the strain all over the surface for the wide specimens.

Fig. 6 presents the stress–strain curves obtained for the narrow and wide specimens. For the wide specimen, there are two curves: one was plotted using the strain measured on the lower section of the specimen and the other the strain measured on the upper section. As can be observed, up to 100 MPa, the stress–strain curves obtained for the two sections are similar. Then, the curve for the upper section slightly

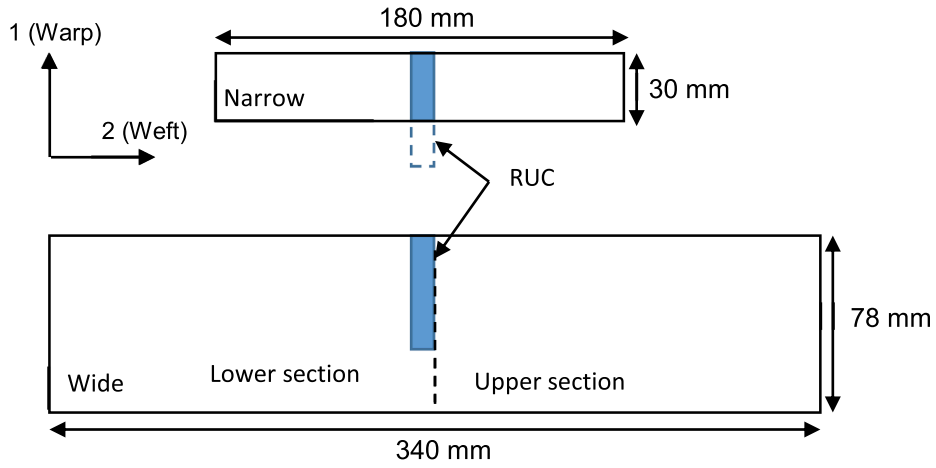

Fig. 5. Specimens geometry for the scale effect study.

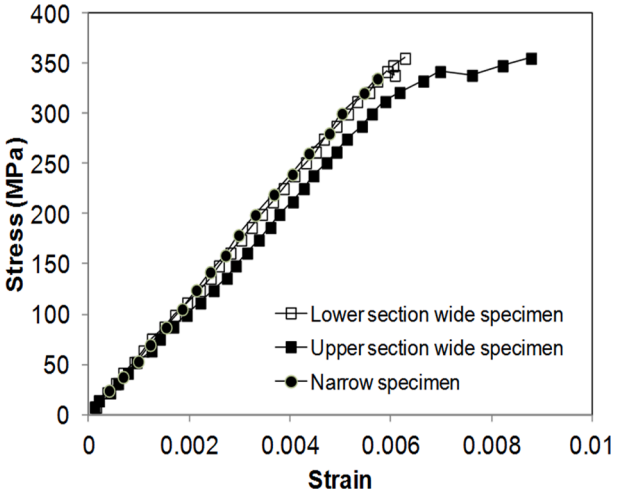

Fig. 6. Scale effect study for the tensile behavior of the 3D angle-interlock woven composite in the weft direction.

deviates probably due to damage occurrence in the top part of the specimen. The stress–strain curve for the narrow specimen is very similar to the one obtained from the lower section of the wide specimen. Therefore, the narrow specimen does not seem to be strongly affected by edge effect as it could have been expected. Based on these results, narrow specimens will be used for the remaining tests as it allows material saving.

Digital image correlation was also used in this test to capture damage mechanisms. Fig. 7 shows (a) the strain field issued from image correlation post-processing and (b) the speckle applied on the specimen. The strain field exhibits high strain concentrations at a few locations. By superposing the strain field with the portion of the specimen where the speckle pattern has been removed, it is possible to identify that the strain concentrations appear where the binding warp tows intersect with the weft ones. They are located on the picture by the identical small areas depicted on the two pictures (a) and (b).

3.1.3. *Test results*

Five specimens were initially tested in both the warp and the weft directions to characterize the material behavior. Unfortunately, one of the tensile tests in the warp direction could not be exploited. Fig. 8 presents the stress–strain curves issued from these tests.

As shown in Fig. 8, the 3D angle-interlock woven composite exhibits a rather linear elastic behavior up to 0.6% strain for both the warp and the weft directions. Above 0.6 % strain, the behavior in the warp direction becomes slightly nonlinear up to final failure. This phenomenon has been previously observed for 3D orthogonal and angle-interlock composites [9–11]. The non-linear behavior is due to damage occurring in the specimens such as matrix cracking. The nonlinearity is much more significant for specimens loaded in the weft direction. As can be observed in Fig. 8b, the stress–strain curve is first linear and then reaches a plateau as progressive failure occurs. These results are in agreement with results obtained in [11] where it was observed that the behavior of a 3D angle-interlock composite in the weft direction was nonlinear with softening damage. The observed differences in the behavior between the warp and the weft directions may be attributed to more important

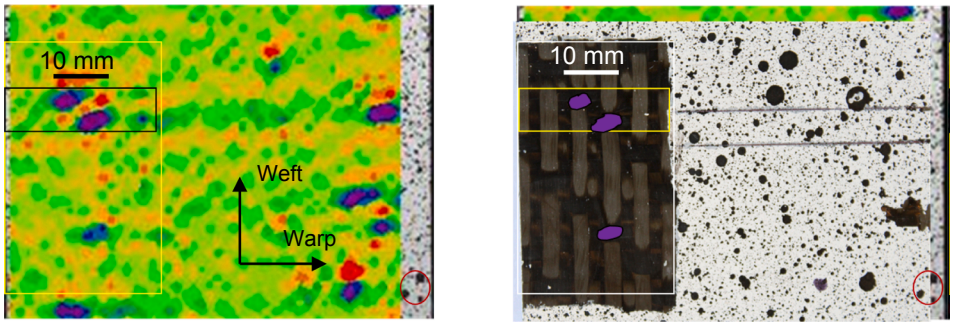

(a) Strain field measured on the specimen surface using DIC

(b) Woven texture below the speckle pattern

Fig. 7. Correlation between the weaving pattern and the high strain concentration areas.

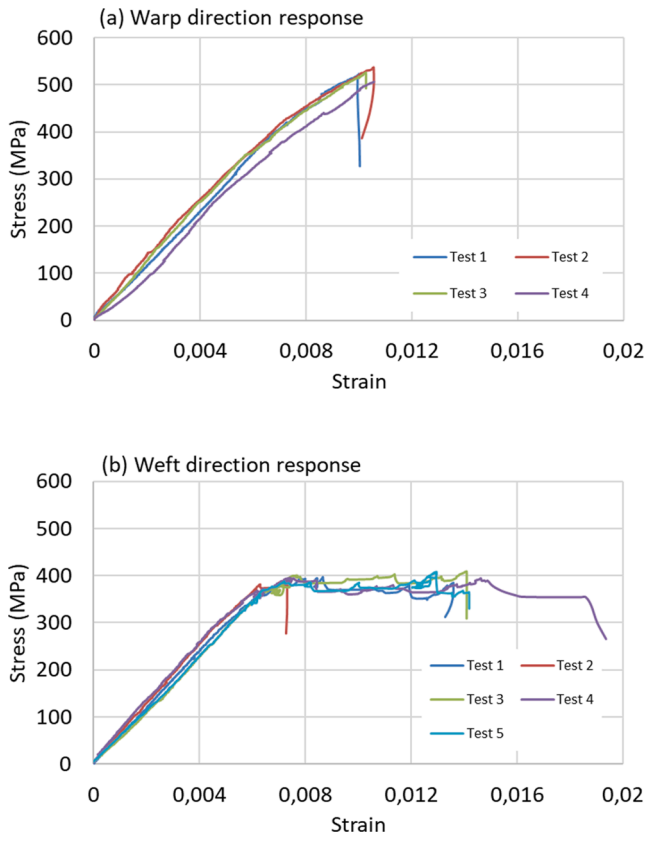

Fig. 8. In-plane tensile stress–strain curves.

interactions between wavy yarns and the matrix when loaded in the weft direction.

Mean values of tensile modulus and strength determined from the experimental tests are presented in Table 1. The 1-, 2- and 3-directions are the warp, weft and through-the-thickness directions, respectively.

3.2. *In-plane shear tests*

3.2.1. *Device and measurements*

A MTS tensile machine equipped with self-locking grips was used. The crosshead speed of the machine was set to 4 mm/min. The crosshead displacement of the machine and the loading force were recorded. A digital image correlation system was again used to measure the strain field on the specimen surface. Five 300 mm-long and 24.5 mm-wide specimens were tested.

Table 1
Mechanical properties of the 3D angle-interlock woven composite.

Test	Direction	Elastic modulus (GPa)	Poisson ratio	Failure stress (MPa)	Failure strain (%)
Tension	1	58.0	–	527	1.05
Tension	2	60.0	0.0688	400	1.4
In-plane shear	1–2	4.61	–	64.6	2.9
Compression	1	44.7	–	397	0.913
Compression	2	47.2	–	443	0.944
Compression	3	11.2	–	–	–
Transverse shear	1–3	2.97	–	40.5	1.4
Transverse shear	2–3	3.29	–	39.7	1.3

3.2.2. *Test results*

Fig. 9 presents the stress–strain curves obtained from the tensile tests performed in the 45°-direction. As shown in the figure, the in-plane shear behavior of the 3D angle-interlock woven composite is non-linear. The initial linear portion of the curve was used to determine the shear modulus. The strength was determined from the ultimate applied force. The mean values of the shear modulus and strength are presented in Table 1.

3.3. *Compressive tests along weft and warp directions*

3.3.1. *Device and measurements*

Compressive tests were performed using a combined loading compression fixture according to the ASTM standard D6641 [25]. The fixture was placed between two compressive platens attached to a MTS universal testing machine. The crosshead speed of the machine was set to 1.3 mm/min. The compressive tests were conducted on 140 mm-long by 12 mm-wide specimens. Back-to-back strain gages (CEA-06-125UW-350) were bonded on the specimen surface along the longitudinal direction as shown in Fig. 10. Scale effect was not studied due to lack of suitable testing device and material. A total of five tests were conducted in the warp and in the weft directions. The percentage of bending in the specimen was determined during testing using:

$$\%\text{bending} = \left|\frac{\varepsilon^1 - \varepsilon^2}{\varepsilon^1 + \varepsilon^2}\right| \times 100 \quad (1)$$

where ε^1 and ε^2 are the strains measured from the two strain gages. The test results were discarded if a bending percentage over 10% was obtained.

3.3.2. *Test results*

Fig. 11 presents the stress–strain curves obtained from the in-plane compressive tests on the 3D angle-interlock woven composite. The strain is the average of the two strain gages measurements. As can be observed, the material presents a rather brittle elastic behavior in compression in both the warp and weft directions with no sign of progressive damage.

Compressive modulus as well as failure stress and strain were determined from the experimental tests and are presented in Table 1. The results of Tests 1 and 5 for the weft direction and Test 5 for the warp direction were not considered in the average computation since the bending percentage was over 10%.

It is interesting to note that the compressive modulus is about 20% less than in tension for both directions. The compressive strength is smaller in the warp direction than in the weft direction, which is probably caused by the important waviness of the through-thickness yarns in this direction.

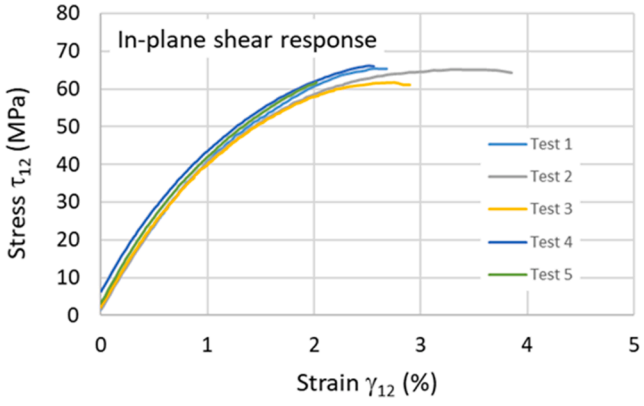

Fig. 9. Stress–strain curve for the tensile test in the 45°-direction.

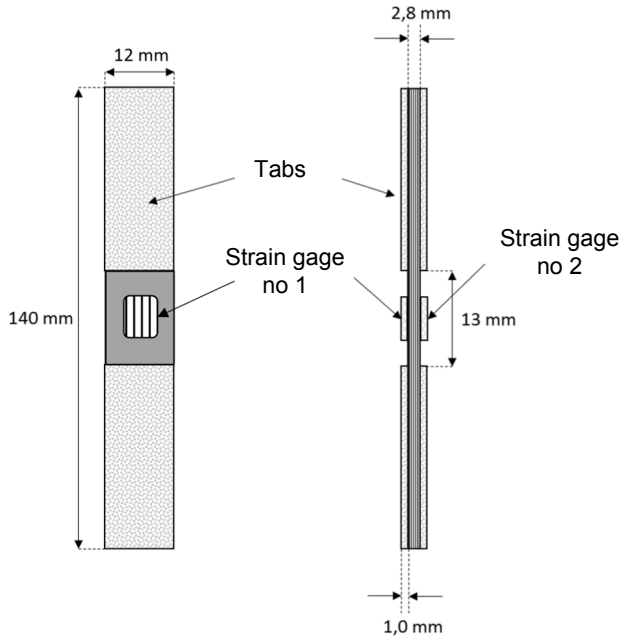

Fig. 10. Specimen configuration used for the in-plane compressive tests.

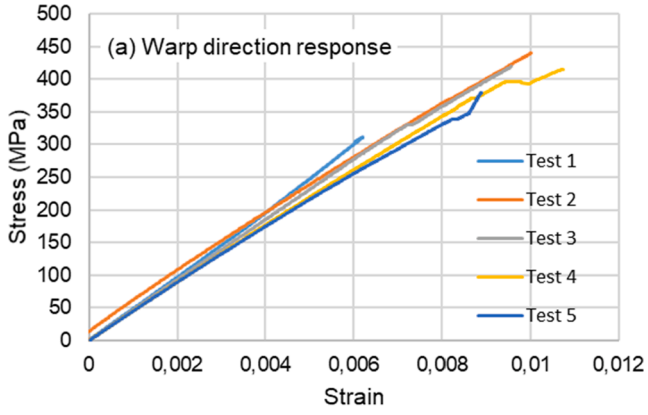

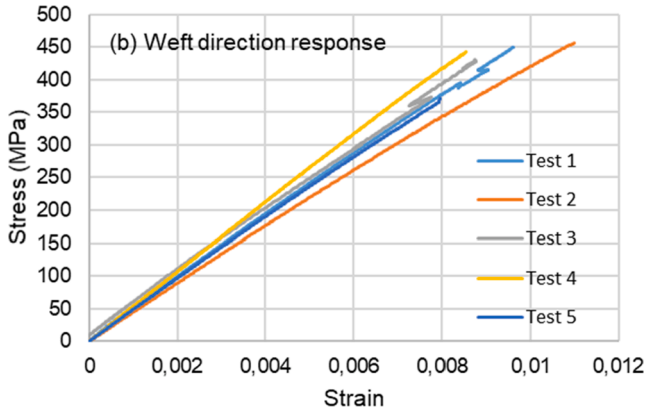

Fig. 11. In-plane compressive stress–strain curves.

4. Through-the-thickness compression tests

4.1. Device and measurements

Conducting the through-the-thickness compression tests on the 3D angle-interlock woven composite was challenging due to the small thickness of the plate (2.8 mm). To overcome this difficulty, the tests were performed on a stack of three 15 mm × 15 mm square samples as shown in Fig. 12. This configuration allows having enough space between the two compression platens to use a digital image correlation system and prevents any barrel effect to occur.

Moreover, the samples were extracted from the initial plate at different locations as shown in Fig. 13. Samples G were cut on a same weft axis than samples D but for two different warp axes. Similarly, samples D and H are cut on the same warp axis but for different weft axis. Therefore, by using samples G_i, D_i and H_i (i = 1 to 9) for the same compression test will allow studying material variability.

The through-the-thickness compression tests were conducted on a MTS universal test machine using compression platens and the compression fixture of the ASTM standard D6641 [25] as shown in Fig. 14a. The compressive fixture was diverted from its initial function and used as a convenient means to apply a uniform compressive force on the stack of samples. This set-up allowed determining the through-thickness elastic modulus of the three samples at the same time using DIC (Fig. 14b). The areas used to average the strains are depicted in Fig. 14c. The areas were selected to be sufficiently away from the sample edges and top and bottom surfaces to obtain a representative average strain.

The crosshead speed of the machine was set to 1.3 mm/min. A total of nine compression tests were conducted using stacked samples $H_i/D_i/G_i$ (i = 1 to 9). Only the elastic behavior was investigated and failure was not reached during testing.

4.2. Test results

Fig. 15 shows the results obtained for one test. After an initial nonlinearity for one of the sample probably due to a non-uniform load introduction, it appears that the 3D angle-interlock woven composite exhibits a linear elastic behavior through-the-thickness direction. Since the compression moduli showed negligible variability between samples H, D and G the compressive modulus was taken as the average of the values obtained for each sample. The through-thickness elastic modulus obtained from these tests is indicated in Table 1.

5. Characterization of transverse shear moduli

Since the 3D angle-interlock composite studied is thick, transverse shear effects may be significant, especially in the case of impact loading. Therefore, the determination of the transverse shear moduli G_{13} and G_{23} is of great interest. In this section, Short Beam Shear (SBS) tests are conducted to identify these properties.

SBS tests consist in subjecting a short composite specimen to three-point bending until failure. The test method has been standardized [26] for continuous or discontinuous fiber –reinforced composite materials. It was developed originally to determine the interlaminar shear strength. In this work, the test method is used in conjunction with a

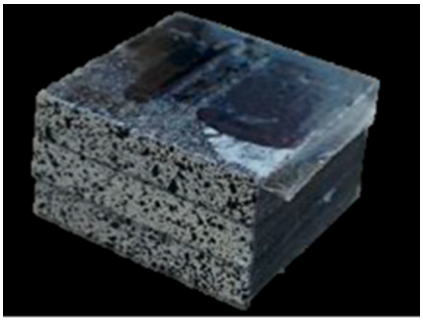

Fig. 12. Stack of three 15 mm by 15 mm square samples.

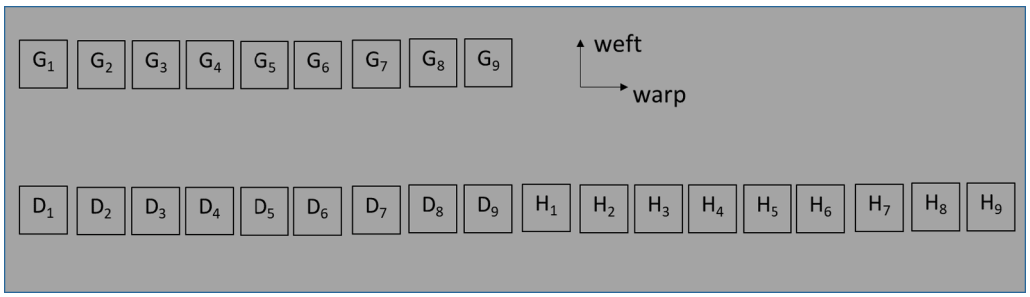

Fig. 13. Sample distribution across the composite plate.

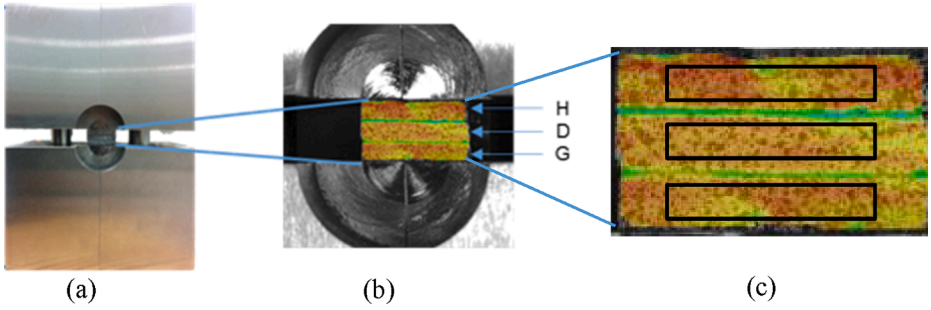

Fig. 14. Experimental set-up for the through-the-thickness compressive tests.

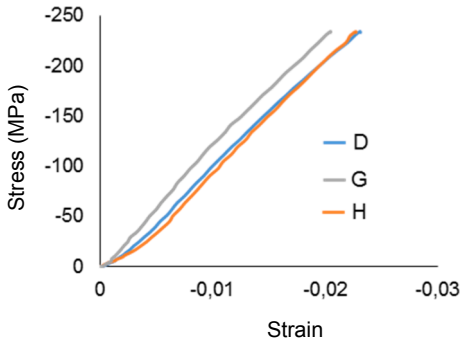

Fig. 15. Through-the-thickness compressive behavior of the 3D angle-interlock woven composite.

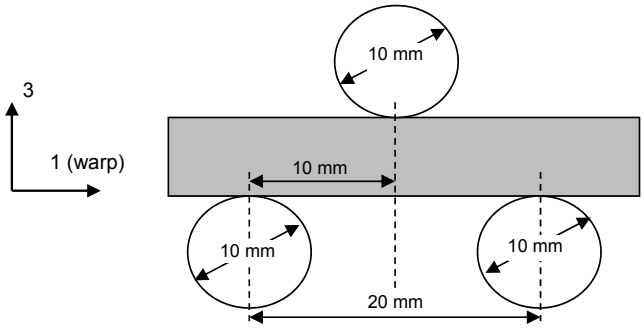

Fig. 16. Three-point bending test configuration.

digital image correlation system to measure the transverse shear strains across the thickness. Therefore, transverse stress–strain curves can be obtained from which transverse shear moduli are determined.

5.1. Test methodology

5.1.1. Device and specimen geometry

Without standard test method for the present 3D angle-interlock woven composite, an existing fixture has been adapted for this study. The fixture configuration is presented in Fig. 16. The specimens were 15 mm wide (out-of-plane dimension in Fig. 16), 2.8 mm thick and the span was 20 mm. This choice follows [26] in which a span-over-thickness ratio ranging between 4 and 10 is recommended to promote shear failure. The specimens were oriented along the warp direction.

Two specimens were tested. For each specimen, cycling loading has been performed until rupture. Table 2 indicates the load level for each cycle. Conducting such a cycling test allows studying the evolution of the transverse shear modulus. The loading speed was 0.2 mm/min. Pictures were taken every two seconds by the digital image correlation system.

Table 2
Bending load cycles for the two specimens.

	Step	Loading (N)	Unloading (N)
Specimen 1	1	400	0
	2	800	0
	3	1200	0
	4	1600	0
	5	2000	0
	6	2400	0
	7	Rupture	
Specimen 2	1	300	0
	2	600	0
	3	900	0
	4	1200	0
	5	1800	0
	6	2400	0
	7	2600	0
	8	Rupture	

5.1.2. Transverse shear stress and strain assessment

From classical beam theory, maximum transverse shear stress can be assessed using:

$$\tau_{13} = \frac{3F}{4bh} \quad (2)$$

where F is the applied force on the loading nose, b is the specimen width and h the specimen thickness.

An example of the results obtained for the shear strain measurements is shown in Fig. 17. The image corresponds to the right half of the specimen. As expected, the strain field displays concentration areas near the loading nose and support. To properly evaluate the transverse shear modulus, shear strain will have to be assessed in an area where it is the most constant. To study the overall strain field distribution beyond the supports, a first area (rectangular zone in Fig. 17) is selected for post-processing. It corresponds to 60% of the entire thickness where the shear strain level is maximum and to the entire half specimen length (respectively H and L in Fig. 17). The analysis of the shear strain field evolution will allow identifying the area where the shear strain is uniform to subsequently reduce the area length for the final post-processing.

5.1.3. *Transverse shear strain evolution on the selected area*

To study the evolution of the shear strain field along the length (L) during testing, the shear strain is averaged over the area height (H) for each image. Fig. 18a shows the shear strain field of Fig. 17 in the vertical position. By averaging the shear strain over the area height (H), a line is obtained for each image. The juxtaposition of the lines obtained for each image allows constructing Fig. 18b. Therefore Fig. 18b represents the resulting average along the area length (in pixels) as a function of image numbers. As can be observed, for each cycle, the shear strain increases, reaches a maximum value and decreases to zero. The transverse shear strain distribution seems to be constant over a region comprised between 550 and 1550 pixels. Based on these results, the retained area for averaging the shear strain field γ_{13} is shown in Fig. 19.

5.2. *Test results*

5.2.1. *Determination of transverse shear modulus G_{13}*

Fig. 20 shows the transverse shear stress–strain curves obtained for the two specimens during the cycling bending loading. The curves do not exhibit too much hysteretic behavior except for the last cycle for which damage probably occurred. The transverse shear modulus is evaluated from the slope of the linear part of the curve during loading and unloading.

5.2.2. *Evolution of transverse shear modulus G_{13} during cycling*

Tables 3 and 4 present the values of G_{13} extracted from the curves of Fig. 20. The values are obtained from both the loading and unloading phases starting at cycle 3 for specimen 1 and cycle 4 for specimen 2. The first cycles for each specimen were not considered because the linear part for these cycles was too small to obtain a reliable value for the slope.

From the tables, it can be noticed that:

- The shear modulus does not change significantly with the number of cycles.
- The G_{13} values extracted from the unloading phases are slightly greater than the ones obtained from the loading phases except for the very last cycle for which damage has occurred.
- The G_{13} values for specimen 2 are slightly smaller than for specimen 1.
- Globally, all G_{13} values are very close.

For specimen 1, the values obtained for the loading and unloading phases of cycles 3, 4, 5 and 6 are averaged to 3.04 GPa. For specimen 2, the values obtained for the loading and unloading phases of cycles 4, 5, and 6 are averaged to 2.89 GPa. The average of these two values is reported in Table 1 as well as the average strength and strain to failure.

The same test method has been applied to determine G_{23}. The final value is reported in Table 1. One can notice that the value for the transverse shear modulus and strength are close to the ones for the 1–3 plane.

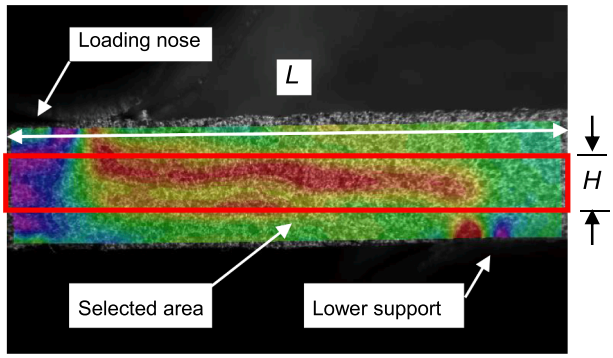

Fig. 17. Transverse shear strain field.

6. Assessment of the elastic properties by ultrasonic method

6.1. *Principle of measurement*

An ultrasonic immersion method is used to identify the full set of elastic stiffness tensor C_{ij} of the material with a single sample and experiment by performing an angular investigation [18,21]. Although for a different kind of materials, the main principles are explained in the international standard ISO 18610 [27]. By inverting the elastic stiffness tensor C_{ij}, (in contracted notation) obtained by ultrasonic propagation, the elastic fourth order compliance tensor, S_{ij} is obtained. The compliance tensor, S_{ij} in contracted notation, then allows to calculate the more commonly used engineering values of elastic properties given by:

$$E_1 = 1/S_{11} \quad E_2 = 1/S_{22} \quad G_{12} = 1/S_{66}$$
$$G_{13} = 1/S_{55} \quad G_{23} = 1/S_{44} \quad (3)$$

The main principles of ultrasonic evaluation have been explained by Roux [28] for the evaluation of the elastic coefficients of homogeneous anisotropic materials. Here after and following convention used in the ultrasonic method, 2 and 3 denote the in-plane directions while 1 indicates the through-the-thickness direction. In order to identify the nine elastic constants C_{ij} which fully describe the elastic behavior of an orthotropic material, the wave propagation velocities are collected in the two accessible principal planes (1–2 and 1–3 planes in Fig. 21) and in a non-principal plane (1-45° plane), described by the bisectrix of axes 2 and 3. The identification in the 1–2 plane gives four elastic constants C_{11}, C_{22}, C_{66} and C_{12}. Three other elastic constants, C_{33}, C_{55} and C_{66}, are obtained in the 1–3 plane. The two remaining coefficients, C_{44} and C_{23}, are identified by propagation in the non-principal 1-45° plane. However, when the material exhibits a tetragonal symmetry, the 1-45° plane becomes a principal plane. It is thus impossible to measure independently the two stiffness coefficients. The value of the in-plane shear modulus C_{44} is obtained from the phase velocity of a shear wave generated with a pair of contact transverse transducers. This value is used together with the 1-45° plane data to simplify and to improve optimization [19]. The dimensions of the tested specimen were 2.8 mm × 98.5 mm × 95.1 mm in the 1-, 2-, and 3-directions, respectively. Its density was 1486 kg.m^{-3}.

6.2. *Results*

The stiffness coefficients obtained by the ultrasonic characterisation with their 90% confidence interval are given under a matrix form by:

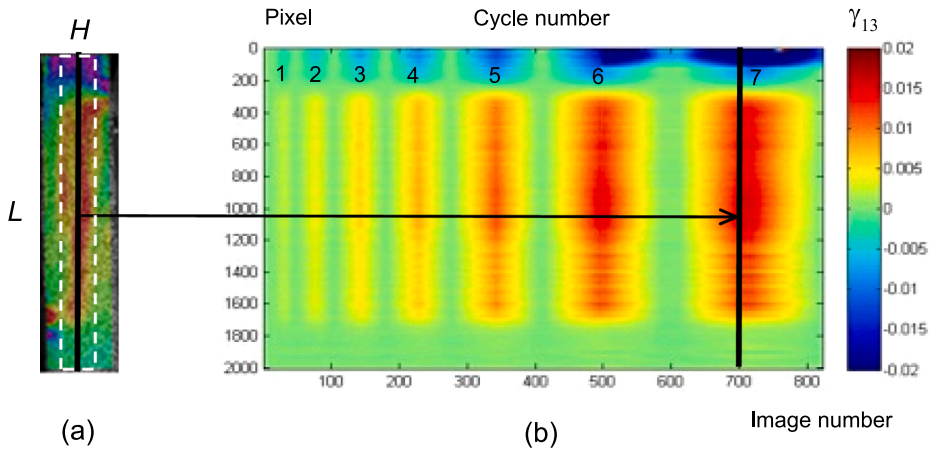

Fig. 18. (a) Shear strain field image in vertical position, (b) Shear strain field evolution along the length *L*.

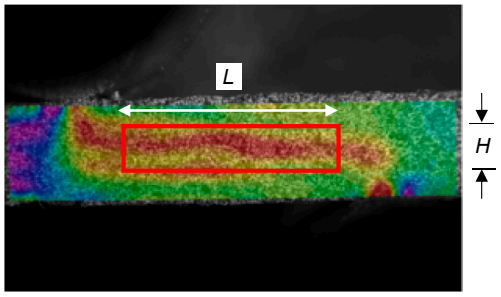

Fig. 19. Final area selected for measurements of γ_{13}.

6.3. Discussion

Table 3
Evolution of the transverse shear modulus G_{13} for specimen 1.

Cycle number	Loading phase	Unloading phase	Difference (%)
3	3.10	3.13	0.967
4	3.09	3.12	0.708
5	3.06	3.06	0
6	2.91	2.90	−0.436

Hereafter standard composite notations are used for discussion. The results obtained by the US technique are very close to the ones obtained from mechanical tests (Table 5). The values of E_3 and G_{23} determined by

$$C_{ij} = \begin{bmatrix} 12.6 \pm 0.1 & 8.0 \pm 2.2 & 7.6 \pm 0.1 & 0 & 0 & 0 \\ & 51.9 \pm 13.9 & 16.6 \pm 10.0 & 0 & 0 & 0 \\ & & 51.4 \pm 1.0 & 0 & 0 & 0 \\ & & & 4.8 \pm 5.1 & 0 & 0 \\ & \text{Sym.} & & & 3.3 \pm 0.6 & 0 \\ & & & & & 3.9 \pm 0.5 \end{bmatrix} \text{(GPa)} \quad (4)$$

After the compliances calculation, the elastic properties are obtained according to Eq. (3) and are presented in Table 5. Note that the 1-, 2-, and 3-axes correspond to the thickness, warp and weft directions, respectively.

US technique show very low scatter and very good correlation with the mechanical tests measurements. Indeed, the difference for E_3 and G_{23} is around 1.8% and 0.3%, respectively. The value of G_{13} shows also very low scatter and a close correlation with the mechanical test measurement. However, the value of G_{13} measured by US technique is slightly higher than G_{23} whereas it is the opposite in the mechanical test

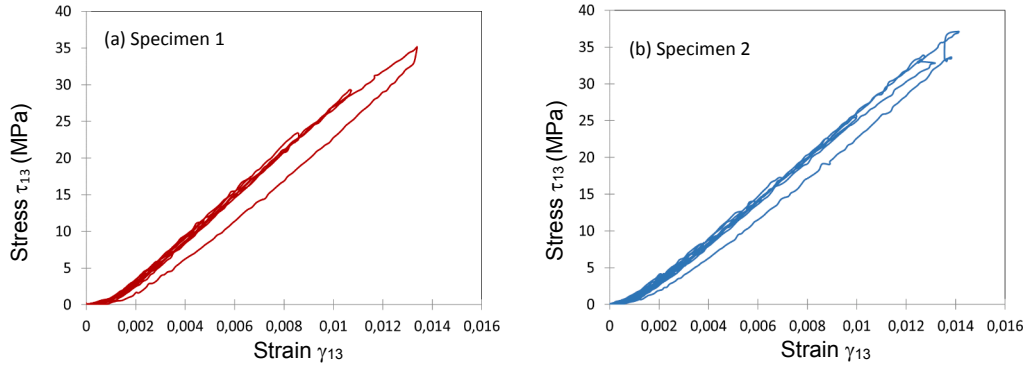

Fig. 20. Transverse shear stress–strain curves until last loading–unloading cycle.

Table 4
Evolution of the transverse shear modulus G_{13} for specimen 2.

Cycle number	Loading phase	Unloading phase	Difference (%)
4	2.91	2.94	1.03
5	2.88	2.91	1.04
6	2.78	2.93	5.39
7	2.90	2.79	−3.79

measurements. Further in-depth investigation would be necessary to explain this trend difference but it is beyond the scope of this study. Finally, it should be underlined that only the US technique is able to estimate values for Poisson ratios v_{31} and v_{32}.

Although other measurements would be necessary to consolidate the tendency, US technique turns out to provide very good estimations of the elastic properties of a 3D angle-interlock textile composite. The technique is particular relevant and convenient to evaluate through-thickness elastic properties that can be difficult to determine using classical mechanical tests due to the small thickness of composite materials. The determination of these through-thickness elastic properties combined with in-plane properties allows identifying the complete elastic stiffness matrix, which is crucial for modeling and evaluating the mechanical behaviour of a composite structure subjected to different loading conditions.

Moreover, the US technique offers the advantage of using only one specimen compared to several specimens of different shapes and sizes for classic mechanical testing and is a non-destructive test method. Such a technique is also suitable for future variability studies.

7. Conclusions and research perspectives

This paper presented the static characterization of a 3D through-the-thickness angle-interlock (or TTAI) woven composite. The objectives were to characterize the full set of mechanical properties (in-plane and out-of-plane), to provide reliable and extensive data to be used in numerical models, and to assess the accuracy of ultrasonic technique to evaluate the elastic properties of 3D composites.

Experimental investigations were conducted to determine in-plane and out-of-plane elastic and failure properties of a 3D angle-interlock composite. In the absence of standard test for such an interlock composite material with a large representative unit cell, various specimen sizes have been considered at first for the tensile tests in the weft direction to assess scale factor effect. No significant effects have been revealed. It would be very interesting to extend this study and investigate scale factor effect for other loading modes. This was not done in this research work due to limited material availability and lack of large fixtures required for this kind of investigation.

Then, in-plane tensile, compression and shear tests have been conducted to determine the elastic modulus in both weft and warp directions and the shear modulus. Compression tests revealed that the compressive modulus was about 20% less than in tension for both warp and weft directions. Besides, the compressive strength was smaller in the warp direction than in the weft direction probably due to the important waviness of the through-thickness yarns in this direction.

Next, the 3D angle-interlock composite was subjected to an original through-the-thickness compression test using a stack of small material pieces taken from different places in a composite plate to take into account variability. DIC was used to assess the through-thickness compressive Young modulus. Then, short-beam shear tests have been developed to assess transverse shear moduli. DIC was used to evaluate the transverse shear strain.

Finally, the through-thickness elastic properties of the 3D angle-interlock composite have been determined using an ultrasonic method. The technique turned out to be relevant to easily obtain good estimates for the through-thickness elastic modulus and transverse shear moduli. The results globally correlate very well with the ones obtained from the mechanical tests. In addition, the ultrasonic method is able to determine through-thickness Poisson ratios. Therefore, US characterization allows identifying the complete elastic stiffness matrix, which is crucial to develop constitutive models aimed at structural design. In addition, it offers the advantages of using only a single specimen and avoiding destructive tests.

To complete this work, variability studies could be done by taking advantage of the US technique. Furthermore, additional tests should be carried out to investigate the damage behavior of such TTAI materials.

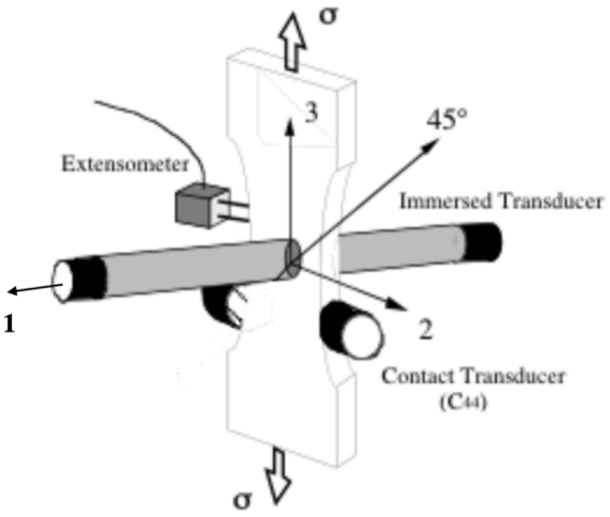

Fig. 21. Specimen instrumented for ultrasonic characterization.

Table 5
Through-thickness elastic properties determined by US technique.

US notation	Standard composite notation	Ultrasounds	Mechanical tests
E_1 (GPa)	E_3 (GPa)	10.8 ± 0.5	11.2 ± 1.14
v_{13}	v_{32}	0.11	–
v_{12}	v_{31}	0.12	–
G_{13} (GPa)	G_{23} (GPa)	3.3 ± 0.6	3.29 ± 0.45
G_{12} (GPa)	G_{13} (GPa)	3.9 ± 0.5	2.97 ± 0.11

Funding

This work was partially funded by the Natural Sciences and Engineering Research Council of Canada.

CRediT authorship contribution statement

F. Dau: Conceptualization, Methodology, Investigation, Resources, Writing – original draft, Writing – review & editing, Visualization, Supervision, Project administration, Funding acquisition. **M.-L. Dano:** Conceptualization, Methodology, Investigation, Resources, Writing – original draft, Writing – review & editing, Visualization, Supervision, Project administration, Funding acquisition. **B. Vérone:** Methodology, Validation, Formal analysis, Investigation, Visualization. **J. Girardot:** Methodology, Supervision. **Z. Aboura:** Methodology, Validation, Formal analysis, Investigation, Resources, Writing – original draft, Visualization. **J.-M. Morvan:** Methodology, Validation, Formal analysis, Investigation, Resources, Writing – original draft.

Declaration of Competing Interest

The authors declare that they have no known competing financial interests or personal relationships that could have appeared to influence the work reported in this paper.

References

[1] Potluri P, Hogg P, Arshad M, Jetavat D, Jamshidi P. Influence of fiber architecture on impact damage tolerance in 3D woven composites. Appl Compos Mater 2012;19(5):799–812.

[2] Cox BN, Dadkhah MS, Morris WL, Flintoff JG. Failure mechanisms of 3D woven composites in tension, compression, and bending. Acta Metall Mater 1994;42(12):3967–84.

[3] Pochiraju K, Chou T-W. Three-dimensionally woven and braided composites. II: an experimental characterization. Polym Compos 1999;20(6):733–47.

[4] Leong KH, Lee B, Herszberg I, Bannister MK. The effect of binder path on the tensile properties and failure of multilayer woven CFRP composites. Compos Sci Technol 2000;60(1):149–56.

[5] Tan P, Tong L, Steven GP, Ishikawa T. Behavior of 3D orthogonal woven CFRP composites. Part I. Experimental investigation. Compos Part A Appl Sci Manuf 2000;31(3):259–71.

[6] Lomov SV, Bogdanovich AE, Ivanov DS, Mungalov D, Karahan M, Verpoest I. A comparative study of tensile properties of non-crimp 3D orthogonal weave and multi-layer plain weave E-glass composites. Part 1: materials, methods and principal results. Compos Part A Appl Sci Manuf 2009;40(8):1134–43.

[7] Ivanov DS, Lomov SV, Bogdanovich AE, Karahan M, Verpoest I. A comparative study of tensile properties of non-crimp 3D orthogonal weave and multi-layer plain weave E-glass composites. Part 2: comprehensive experimental results. Compos Part A Appl Sci Manuf 2009;40(8):1144–57.

[8] Gerlach R, Siviour CR, Wiegand J, Petrinic N. In-plane and through-thickness properties, failure modes, damage and delamination in 3D woven carbon fibre composites subjected to impact loading. Compos Sci Technol 2012;72(3):397–411.

[9] Dai S, Cunningham PR, Marshall S, Silva C. Influence of fibre architecture on the tensile, compressive and flexural behavior of 3D woven composites. Compos Part A Appl Sci Manuf 2015;69:195–207.

[10] Cox BN, Dadkhah MS, Morris WL. On the tensile failure of 3D woven composites. Compos Part A: Appl Sci Manufact 1996;27(6):447–58.

[11] Warren KC, Lopez-Anido RA, Goering J. Experimental investigation of three-dimensional woven composites. Compos Part A Appl Sci Manuf 2015;73:242–59.

[12] Castaneda N, Wisner B, Cuadra J, Amini S, Kontsos A. Investigation of the Z-binder role in progressive damage of 3D woven composites. Compos Part A Appl Sci Manuf 2016;98:76–89.

[13] Saleh MN, Yudhanto A, Potluri P, Lubineau G, Soutis C. Characterizing the loading direction sensitivity of 3D woven composites: Effect of z-binder architecture. Compos Part A Appl Sci Manuf 2016;90:577–88.

[14] Wang Y, Zhao D. Effect of fabric structures on the mechanical properties of 3-D textile composites. J Ind Text 2006;35(3):239–56.

[15] Gras R, Leclerc H, Roux S, Otin S, Schneider J, Périé JN. Identification of the Out-of-Plane Shear Modulus of a 3D Woven Composite. Exp Mech 2012;53(5):719–30.

[16] Fishpool DT, Rezai A, Baker D, Ogin SL, Smith PA. Interlaminar toughness characterisation of 3D woven carbon fibre composites. Plast Rubber Compos 2013;42(3):108–14.

[17] Saleh MN, Soutis C. Recent advancements in mechanical characterisation of 3D woven composites. Mech Adv Mater Mod Process 2017;3(12).

[18] Baste S, Hosten B. Evaluation de la matrice d'élasticité des composites orthotropes par propagation ultrasonore en dehors des plans principaux de symétrie. Revue Phys Appl 1990;25(2):161–8.

[19] Hosten B. Stiffness matrix invariants to validate the characterization of composite materials with ultrasonic methods. Ultrasonics 1992;30(6):365–71.

[20] Hood JA, Mignognat RB. Determination of elastic moduli in anisotropic media from ultrasonic contact measurements. Ultrasonics 1995;33(1):45–54.

[21] Audoin B, Baste S. Ultrasonic Evaluation of Stiffness Tensor Changes and Associated Anisotropic Damage in a Ceramic Matrix Composite. J Appl Mech 1994;61(2):309–16.

[22] ASTM Standard D6856, Standard Guide for Testing Fabric-Reinforced "Textile" Composite Materials, ASTM International, West Conshohocken, PA.

[23] Dau F, Dano M-L, Duplessis-Kergomard Y. Experimental investigations and variability considerations on 3D interlock textile composites used in low velocity soft impact loading. Compos Struct 2016;153:369–79.

[24] Boussu F, Cristian I, Nauman S. General definition of 3D warp interlock fabric architecture. Compos Part B 2015;81:171–88.

[25] ASTM standard D6641, Standard Test Method for Compressive Properties of Polymer Matrix Composite Materials Using a Combined Loading Compression (CLC) Test Fixture, ASTM International, West Conshohocken, PA.

[26] ASTM Standard D2344, Standard Test Method for Short-Beam Strength of Polymer Matrix Composite Materials and Their Laminates, ASTM International, West Conshohocken, PA.

[27] ISO 18610, Fine ceramics (advanced ceramics, advanced technical ceramics)—Mechanical properties of ceramic composites at room temperature—Determination of elastic properties by an ultrasonic technique.

[28] Roux J. Elastic Wave Propagation in Anisotropic Materials. Proc IEEE Ultrasonics Symposium. Honolulu December 1990:1065–73.